Supplementary Information

Experiment on topological-like transport enabled by nonreciprocal mechanical circulators

Jinliang Wang[1], Qingxiang Ji[1*], Brahim Lemkalli[1], Jingyi Zhang[3], Richard Craster[4], Johan Christensen[3], and Muamer Kadic[1,2]

[1]Université Marie et Louis Pasteur, SUPMICROTECH, Institute FEMTO-ST, Besançon, 25000, France

[2]Institut Universitaire de France, 103 boulevard Saint-Michel, 75005 Paris, France

[3]IMDEA Materials Institute, 28906, Getafe, Madrid, Spain

[4]UMI 2004 Abraham de Moivre-CNRS, Imperial College London, SW7 2AZ, London, UK

[*]To whom correspondence should be addressed; E-mail: qingxiang.ji@femto-st.fr

Materials and Methods

Design and fabrication

The system consists of circulators. Each circulator is comprised of three beams and three hinges. The beams are made by laser cutting out of steel. The geometry parameters of the beams are: overall length 145 mm, length of the deformed part 105 mm, height 10 mm, and thickness 0.5 mm. They are cut by laser to locate slots and screw holes. There are three types of beams as defined by the position of locating slots: top, middle, and bottom, as shown in Fig. S1(a). The sleeves of the hinge consist of aluminum blocks made by 3D printing and a steel plate made also by laser cutting, as shown in Fig. S1(b). The steel plates consist of a ring wrapping the axle and two pairs of locating pins (inset panel), determining the relative position with the beams. The radius of the hinge is 20 mm and the height is 18 mm. Corresponding to the beams, there are also three types of sleeves. Both the locating slots on beams and the locating pins on sleeves are drilled by laser cutting, so that they can be precisely assembled together, as shown in Fig. S1(c). This makes the length of the deformed part of all beams uniform. The beams are

clamped on sleeves by pressing plates, as shown in Fig. S1(d). In Fig. S1(e), we show the circulators to be assembled at different locations.

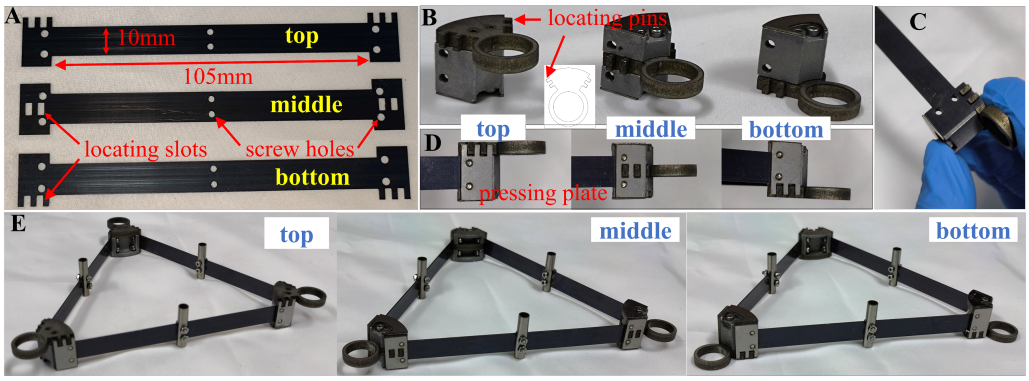

Figure S1: **Design of the circulator.** **(a)** The three types of beams: top, middle, and bottom types, as defined by the position of locating slots. They are cut by laser to locate slots and to screw holes. **(b)** The corresponding sleeves of the hinge, which consist of aluminum blocks made by 3D printing and a steel plate by laser cutting. The steel plates form a ring wrapping the axle and two pairs of locating pins (inset figure), determining the relative position with beams. **(c)** The locating slots on beams and the locating pins on sleeves are both manufactured by laser cutting, so that they precisely match in the assembly process. **(d)** The pressing plates, manufactured by laser cutting, are connected with sleeves by the screw. The beam is sandwiched between the pressing plate and the sleeve to be fixed. **(e)** The three types of circulators used in this work.

The axles of hinges and plates are manufactured using CNC machining with copper and they are inlaid with graphite which makes them self-lubricating. Two copper plates (we only show one plate in the figures) hold the sleeve in the middle to constrain its displacement along the vertical direction and leave an interval gap of 0.5 mm to make the sleeve move freely. The radius of the axle is 6 mm and the height is 55 mm. The beams are compressed from two ends by 5 mm to form the second-bucklingd state, as shown in Fig. S2(a). It is unavoidable that three circulators share one copper axle of the hinge. The three types of sleeves of hinge can coordinate space: the rings of the sleeve of hinge are at the top, middle, and bottom positions, respectively. They wrap the same axle but don't contact each other, as shown in Fig. S2(b).

The two adjacent circulators are arranged vertically and connected by a pin joint

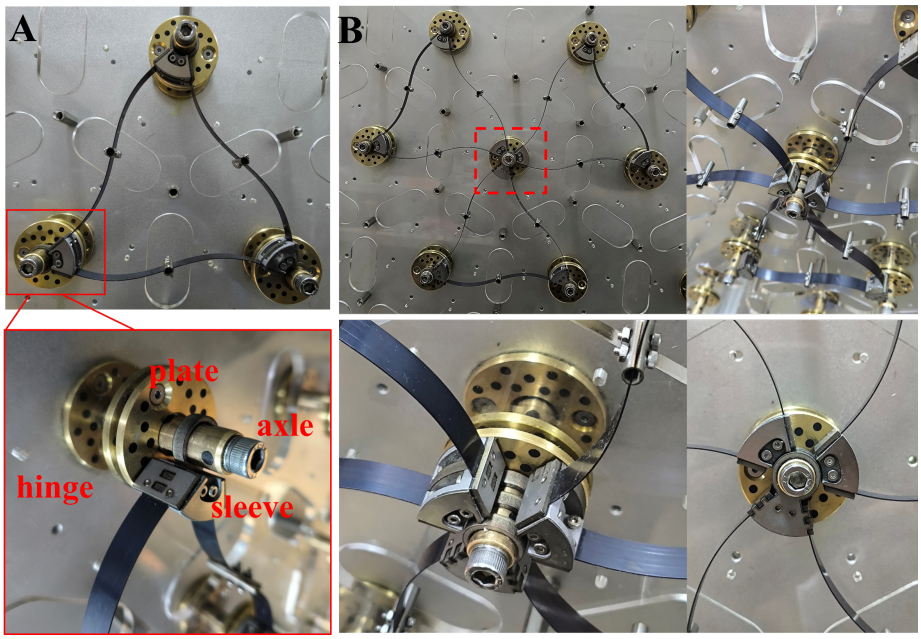

Figure S2: **Assembling of the circulators.** **(a)** The overall view and partial enlarged view of the hinge. The copper axle and sleeve assembly constitutes the hinge. Two copper plates (only one plate is shown in the figure) hold the sleeve in the middle to restrict the displacement along the vertical direction, and leave an interval gap of 0.5 mm to enable the sleeve move freely. Both the copper plates and the shaft are inlaid graphene block for lubrication. **(b)** Three circulators that share the same copper axle. The design of the three types of circulators can't interfere with each other, although they share the same copper axle.

located at the midpoint of the beams. The pin joint consists of two axles and a sleeve. Each axle is a thin steel tube (outer radius 2.5 mm, thickness 0.5 mm, and length 23 mm) installed at the midpoint of the beams in the two adjacent circulators, as shown in Fig. S3(a).

We use a laser engraving machine to cut four circular holes and two rectangular holes in each thin steel tube (bottom figures). The rectangular holes clamp the beam, while the circular holes allow the screws to pass through and to be connect with the beam midpoint (upper figure). The engraved pattern is asymmetric along the vertical direction, with the longer portion designed to be wrapped by sleeves.

The sleeve of the pin joint is a larger thin steel tube (inner radius 2.6 mm, thickness 0.4 mm, and length 19.5 mm) that encloses the two axles. The composition and assembly of the pin joint are illustrated in Fig. S3(b).

Since adjacent circulators are connected by a pin joint, the overall structure naturally forms two layers, as shown in Fig. S3(c). Each circulator is connected vertically to three other circulators by three pin joints, as shown in Fig. S3(d). Consequently, the topological-like structure resembles the lattice of graphene, where all cells are interconnected. Notably, six circulators share the same copper axle across the two layers, as shown in Fig. S3(e).

In the edge state demonstration, we designed a hard wall fabricated by 3D printing with polylactic acid (PLA), as shown in Fig. S4(a). The wall includes two T-slots for positional adjustment. The supporting column contacts the circulator to reflect the signal, while the notch on the column provides clearance to avoid interference, as shown in Fig. S4(b). A steel tube was designed to connect with the hard wall. This tube is assembled at the midpoint of the beam and has a shape similar to the axle of the pin joint, except that it is symmetric along the vertical direction, as shown in Fig. S4(c).

The topological-like structure consists of 54 cells in Interface A (Z-shaped domain wall) and Interface B (circle-shape domain wall), and 42 cells in Interface C (external edge). The overall size of the assembled sample is 830 mm $\times$ 800 mm $\times$ 70 mm. The samples are mounted on an aluminum substrate and covered with acrylic plates between the two layers and on top of the sample, which are sufficiently transparent for optical imaging. Holes are drilled into the acrylic plates to avoid interference with the pin joints, as shown in Fig. S5(a,b).

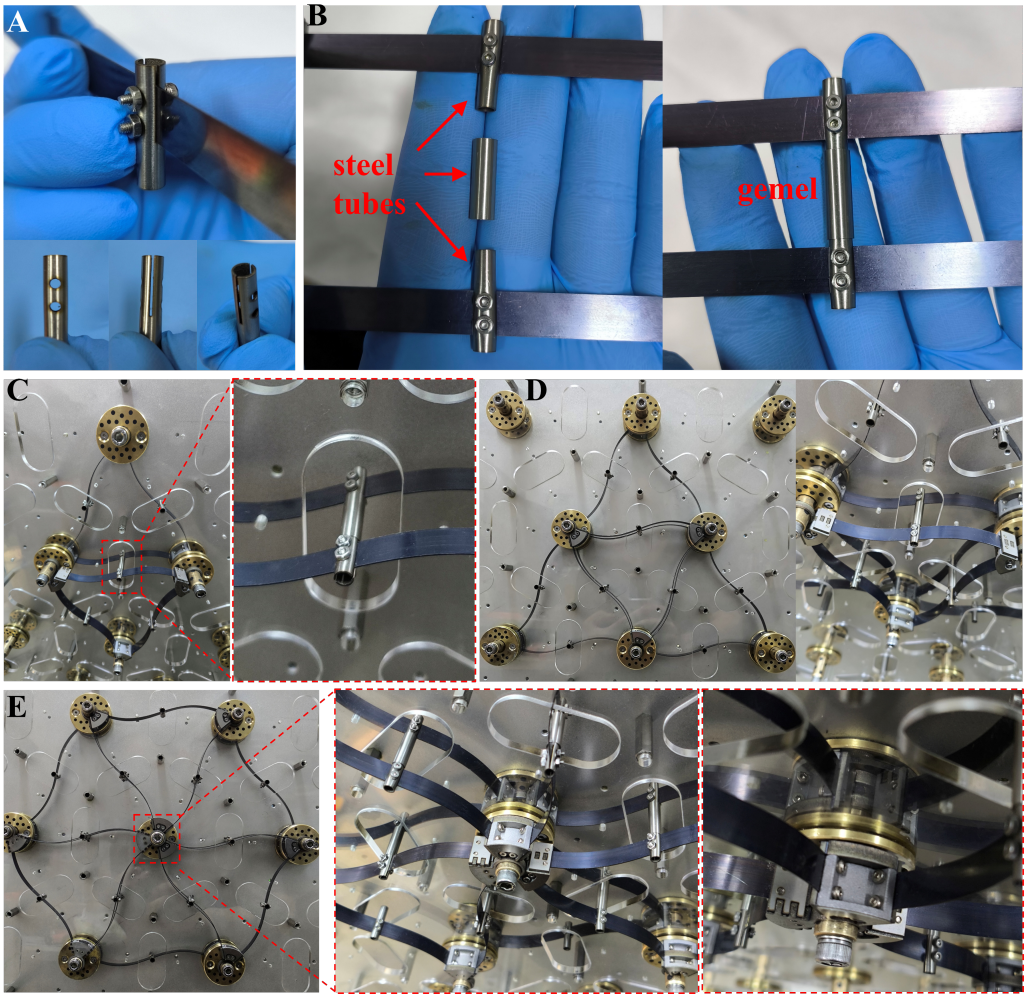

Figure S3: **Design of the connection nodes between beams across different layers.** **(a)** Axle of the pin joint. A laser engraving machine is used to cut four circular holes and two rectangular holes into a thin steel tube (bottom figures). The rectangular holes clamp the beam, while the circular holes allow screws to pass through and connect to the beam midpoint (upper figure). The engraved pattern is asymmetric along the vertical direction, with the longer portion designed to be wrapped by the sleeve. **(b)** Composition of the pin joint. Adjacent circulators are connected by a pin joint: a larger steel tube (upper figure) wraps the two axles from two circulators to form the pin joint (bottom figure), naturally creating a two-layer structure. **(c)** Connection between adjacent circulators and a pin joint. **(d)** Each circulator connects to three others through three pin joints. **(e)** Six circulators share the same copper axle across two layers, ensuring interconnection.

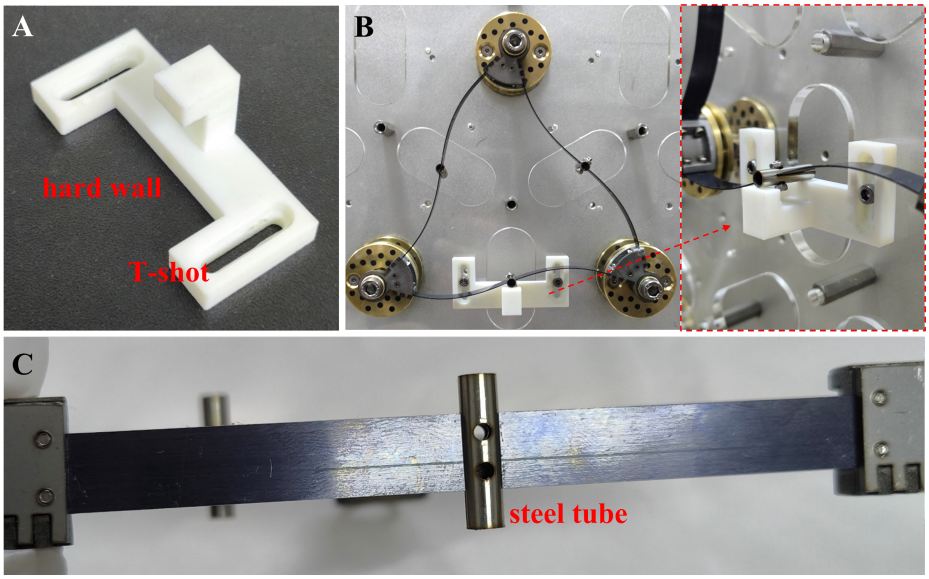

Figure S4: **Design of the hard wall and circulator on the edge.** **(a)** Hard wall fabricated by 3D printing with polylactic acid (PLA). It includes two T-slots for positional adjustment. The supporting column contacts the circulator to reflect the signal, and the notch on the column provides clearance. **(b)** Circulator in contact with the hard wall. **(c)** Steel tube designed to connect with the hard wall. The tube is assembled at the midpoint of the beam and has a shape similar to the axle of the pin joint, except that it is symmetric along the vertical direction.

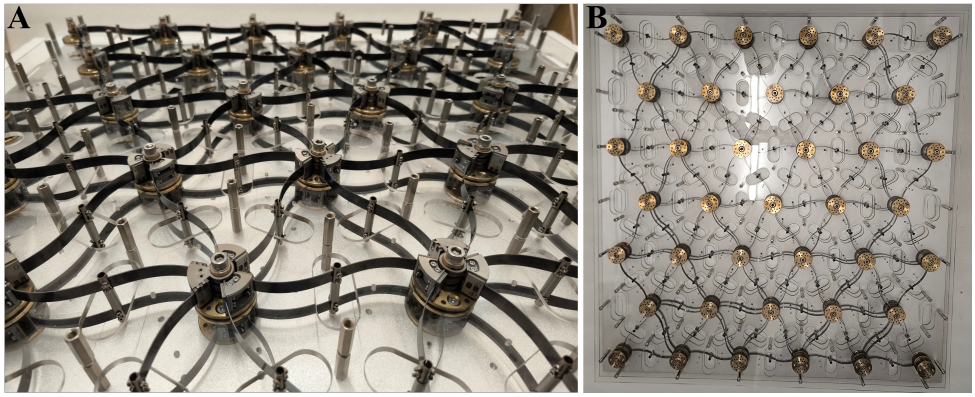

Figure S5: **Overall view of the topological-like insulator.** **(a)** Axonometrical view (removing the top acrylic plate). **(b)** Top view.

Finite element analysis

The simulation of circulators and topological-like insulators was performed in ABAQUS 2021. The structure was modeled using deformed shell elements of type S4R for circulators and deformed beam elements of type B31 for lattice. The material parameters of the spring steel beams are: elastic modulus $E = 205$ GPa, Poisson's ratio $\mu = 0.25$, and density 7.85 g/cm^3. The geometric parameters are identical to the design. Nonlinear implicit dynamics were employed to compute the propagation of transtion wave. The pin joint was simulated by imposing constraint equations between two corresponding points, restricting all degrees of freedom except for rotation. Boundary conditions in the simulations matched those of the experiments. Each undeformed beam was initially pre-compressed by 5 mm into the second-buckling state, after which an input displacement was imposed at the input point. In the edge state demonstration, contact constraints were applied between points on the edge of the structure and the hard walls to obtain the corresponding deflection.

The simulation is conducted based on the assumption that the material property of the structure is liner elastic. This assumption requires the local strain of the beams to be small throughout, even when they undergo a finite deformation during the shape-transition. The FEA based von Mises stress and strain are shown in Fig. S6. The strain maps shows that local maximum principal strain remains below 0.4%, validating the assumption of a small local strain. Therefore, we safely conclude that the overall response adheres to linear elasticity.

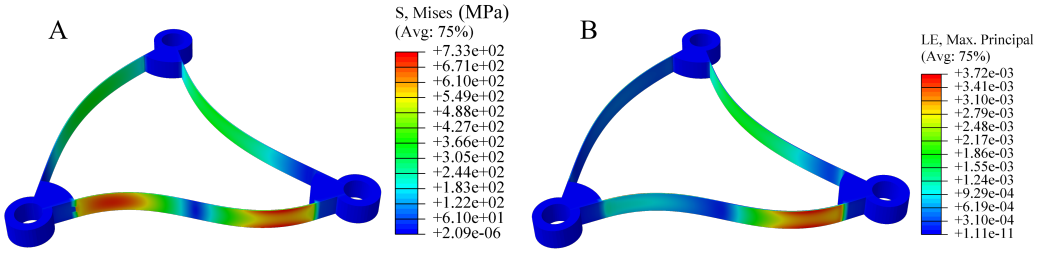

Figure S6: **Demonstration of linear elasticity.** (a) Von Mises stress and (b) strain are obtained by Finite Element analysis. Small deformation of the structural elements (no larger than 0.4%) safely demonstrates that the deformation process is in its linear regime.

Experimental Setup

The high-speed camera used in the experiments is a Revealer X113M, with a frame rate of 3003 fps and a resolution of 1024×1280. The sample was placed vertically on a metal supporting frame to facilitate imaging, as shown in Fig.3c. A slide rail was employed to adjust the relative position between the camera and the sample. Momentum was generated by an actuating plunger driven by an electric motor, with a speed defined as 90 $\mathrm{mm/s}$. The entire system was placed in a dark environment, illuminated by an intense light source to ensure clear imaging of the sample.

The propagation of the transition wave was recorded by the high-speed camera. Digital Image Correlation (DIC) analysis was then applied to extract the deformation of the beams.

The stability of circulators

Remarkably, three beams that are intrinsically unstable in the second-mode buckling state remain stable once interconnected into a ring. This stabilization mechanism originates from the mutual mechanical constraints among the three beams, which collectively suppress their individual instability tendencies. For Beam 3, the counterclockwise moments applied at both ends (Fig.S7) increase its internal stress and consequently raise its strain energy, as shown in Fig.S8c. For Beam 2, the moment transferred from Beam 3 constrains the rotation of Hinge *C*, resisting the deformation of Beam 2 and increasing its elastic potential energy, as shown in Fig.S8b. For Beam 1, the moments applied at Hinges *A* and *B* oppose its deformation direction, resulting in smaller rotation angles $\Delta\alpha_{\mathrm{A}}$ and $\Delta\alpha_{\mathrm{B}}$ than $\Delta\alpha_{\mathrm{L}}$ and $\Delta\alpha_{\mathrm{R}}$ (Fig. 1a) and raising its strain energy during the initial stage, as illustrated in the right panel of Fig. S8a. Overall, the strain energy stored in all three beams increases during the initial stage (Fig.S8), thereby stabilizing the circulator and enabling its practical implementation.

Topological-like transport along Z-shaped domain wall

To validate the ability of the transition wave to turn around extremely sharp corners with 180°, a Z-shaped domain wall was designed, as shown in the left panel of Fig.S9a. The transition wave is excited at the upper-right port of the lattice and propagates steadily along the predefined pathway, eventually exiting through the output port, as shown in the right panel of Fig.S9a. During propagation, the transi-

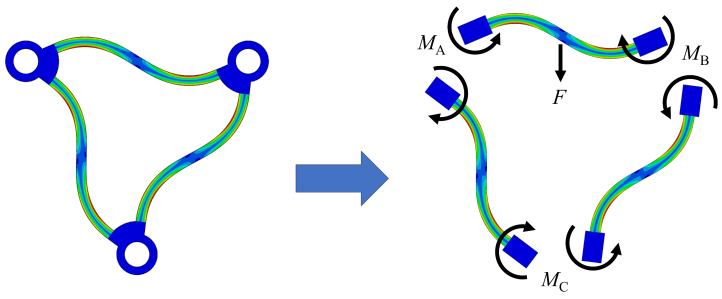

Figure S7: **Force analysis Diagrams.** Force analysis diagrams of each beams in circulator

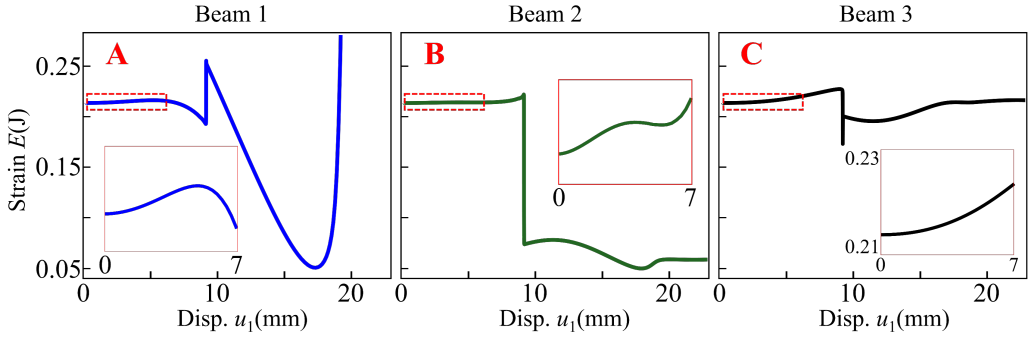

Figure S8: **Strain Energy of each beams.** The strain energy of Beam 1 (**a**), 2(**b**) and 3(**c**) as a function of input displacement u_1.

tion wave exhibits key characteristics of topological-like transport, including edge localization, robustness against sharp corners, and pronounced non-reciprocity. The deformation field remains strictly confined to the domain wall, while no observable displacement occurs at the bulk nodes, further demonstrating the strong localization of the transport process, as shown in the right panel of Fig.S9a. Notably, the transition wave propagates smoothly along the domain wall at a almost constant velocity and successfully detours two extremely sharp corners with 180° without backscattering, highlighting its robustness against abrupt changes in the propagation pathway, as shown in Fig.S9b. The experimental results show good agreement with the numerical simulations, as shown in Fig.S9c. Furthermore, non-reciprocity is experimentally validated by applying the displacement excitation at the opposite port, which redirects the transition wave along a completely different pathway rather than retracing the original route, as shown in Fig.S9d.

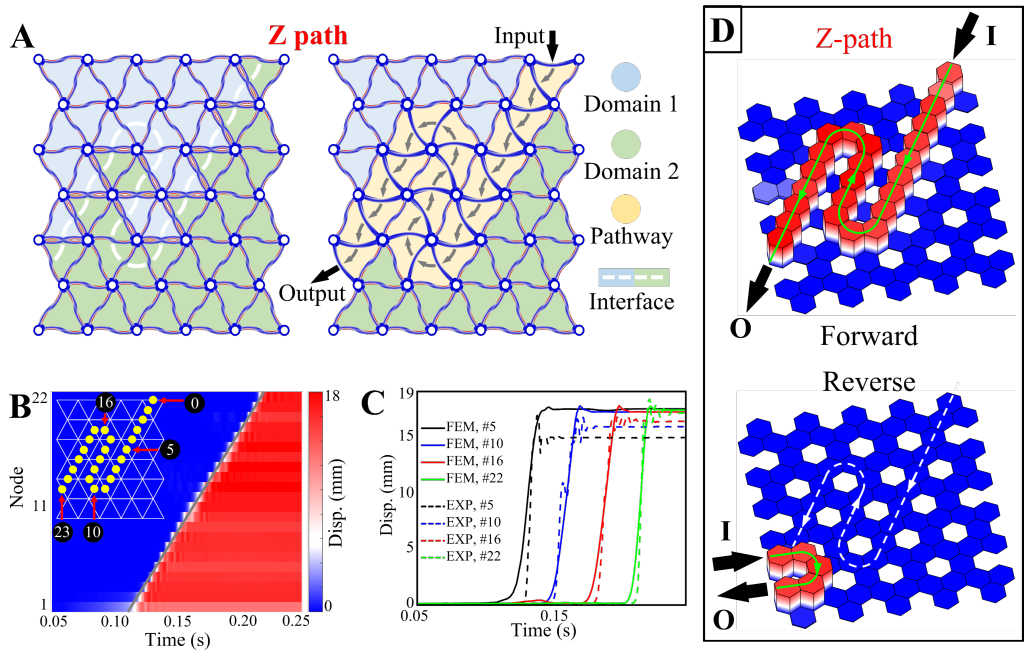

Figure S9: **The topological-like transport localized to domain wall with Z shape. a** A Z-shaped domain wall composed of circulators with left-handed (blue domain) and right-handed (green domain) chiralities, containing two extremely sharp corners with 180°. A displacement signal transports forward (yellow region) along the domain wall and finally exits from the output port. **b** Experimentally measured spatiotemporal displacement diagram of forward transport along the domain wall. **c** The profile of forward transition wave extracted from typical nodes. Simulated and experimental results agree well. **d** Excitation from the opposite port redirects the transition wave along a completely different pathway (lower panel), demonstrating non-reciprocity.